AIMS Mathematics, 11(5): 14617–14640.
DOI: 10.3934/math.2026599
Received: 20 January 2026
Revised: 29 April 2026
Accepted: 11 May 2026
Published: 25 May 2026

https://www.aimspress.com/journal/Math

Research article

From optical solitons to chaos: stochastic dynamics in nonlinear Schrödinger systems

Saad Althobaiti[1] **and Hamood Ur Rehman**[2,*]

[1] Department of Science and Technology, University College Ranyah, Taif University, Ranyah 21975, Saudi Arabia

[2] Department of Mathematics, University of Okara, Okara, Pakistan

* **Correspondence:** Email: hamood84@gmail.com.

Abstract: This paper considers the stochastic nonlinear Schrödinger equation with Brownian motion for the representation of noise effects in the propagation of waves. Using the modified Sardar sub-equation method, exact solutions of the solitons and periodic type are constructed. The effect of stochastic perturbation on the solutions is studied revealing the formation of deformations and instabilities. The chaotic nature of the system is further verified under the effects of sinusoidal, cosine, hyperbolic, and Gaussian perturbations through numerical experiments. Phase diagrams and time series show a very complex non-periodic pattern. Sensitivity to the initial condition proves that the solution is highly sensitive to changes in the initial values.

Keywords: optical solitons; phase portraits; Brownian motion; modified Sardar subequation method
Mathematics Subject Classification: 35Q51, 35Q55

1. Introduction

Nonlinear partial differential equations (NLPDEs) are fundamental in describing complex wave phenomena in a broad range of fields such as fluid mechanics, physics, biology, and chemistry. Seeking exact analytical solutions to NLPDEs continues to be a fascinating field of study because of its theoretical value and application importance. Perhaps one of the most fascinating families of solutions to NLPDEs are solitons or solitary waves. These waveforms are characterized by their excellent resistance to both speed and shape, even after undergoing interactions with other waves. Solitons not only have an elegant mathematical quality, but also produce realistic and correct descriptions of some physical systems involving a balance of nonlinearity and dispersion [1–3]. Recently, novel solution approaches have been introduced, including the Sardar sub-equation method [1, 4], Kudryashov's method [5, 6], the Bernoulli sub-ODE method [7, 8], the mapping method [9–11], Jacobi's elliptic

function [12,13], the extended hyperbolic function method [14–16], and the ϕ^6-expansion method [17]. These methods significantly contribute to the advancement of nonlinear wave research, providing further insight into the dynamics of optical solitons and their application in modern communication systems.

A stochastic process, or random process, is a mathematical construct applied to represent the probabilistic change of a system or quantity over time. It is basically an indexed family of random variables, which capture the underlying randomness inherent in dynamic systems. Stochastic processes are basic instruments in a vast array of fields such as probability theory, statistics, finance, physics, and engineering. They offer a strong tool for modeling and analyzing uncertainty in complicated real-world processes. They can be divided into discrete-time and continuous-time processes, with a number of popular examples like Brownian motion (Wiener process), geometric Brownian motion, Poisson processes, autoregressive models, Gaussian processes, and Markov processes, each of which is a fundamental model in theoretical study and applications.

The nonlinear Schrödinger equation (NLSE) is a basic partial differential equation describing the evolution of a complex wave envelope in nonlinear and dispersive media. It finds important applications in many physical contexts including optical fiber communication, plasma physics, water wave theory, and Bose-Einstein condensates [18–20]. The NLSE is able to represent the subtle interplay between nonlinearity and dispersion, allowing it to model localized wave structures like solitons waves that conserve their form as they travel at a fixed speed. Yet, in most real-world systems, perfect conditions are never encountered, and random fluctuations or noise due to environmental perturbations, thermal influences, or quantum fluctuations become important factors in determining wave behavior. To explain such randomness, the NLSE is generalized to include stochastic components, and the stochastic nonlinear Schrödinger equation (SNLSE) is formulated. The SNLSE contains noise terms, which are generally represented by stochastic processes like Brownian motion, and can be used to investigate how randomness and uncertainty influence soliton stability, wave coherence, and long-term behavior. This stochastic extension gives a more realistic and complete model for wave propagation in noisy, complex environments, and is especially useful in fields such as fiber optics and nonlinear quantum systems where fluctuations cannot be ignored. The SNLSE considered in this study is given by [21]

$$iU_t + \frac{1}{2}U_{xx} - a\delta U - \lambda|U|^2U + \rho UB_t = 0, \tag{1.1}$$

where every term holds different physical meaning. The expression iU_t signifies the temporal evolution of the complex wave envelope $U(x,t)$. The second expression $\frac{1}{2}U_{xx}$ explains group velocity dispersion, indicating how different frequency components of the wave propagate over time, a distinctive feature in pulse propagation in optical fibers. The third term $-a\delta U$ refers to either a linear potential or damping, depending on the application, where a is a scale constant and δ can refer to a spatially varying potential or a damping coefficient responsible for energy loss. The nonlinear interaction is accounted for by $-\lambda|U|^2U$, representing the cubic Kerr-type nonlinearity occurring in nonlinear media, resulting in effects such as self-phase modulation and soliton formation. Lastly, the stochastic term ρUB_t accounts for multiplicative noise via the Brownian motion B_t, which models random perturbations from the ambient environment. This is critical to modeling realistic systems affected by thermal fluctuations, material inhomogeneities, or quantum noise. The coefficient ρ measures the strength of these stochastic

effects. Collectively, Eq (1.1) controls the evolution of optical or quantum waveforms in a nonlinear, dispersive, and noisy medium.

For deriving precise analytical solutions of the nonlinear system, we use the modified Sardar sub-equation method (MSSEM) [22], a robust algorithm for solving stochastic models and NLPDEs. MSSEM is an advanced upgrade of the classical Sardar method, which builds traveling wave solutions by truncating the initial equation into an ordinary differential equation (ODE) using an appropriate wave transformation. The technique assumes a polynomial ansatz with solutions of an auxiliary sub-equation, whose form is selected with care to equalize the nonlinear and dispersive terms in the reduced ODE. Substitution of the ansatz into the transformed equation, followed by an equating of coefficients, produces a set of algebraic equations, which is solved to define the exact nature of the solution. The enhanced framework enhances flexibility and supports wider solution structures, such as soliton, periodic, singular, and rational profiles. In the stochastic NLSE case, the use of MSSEM enables the systematic derivation of explicit solutions for the real and imaginary parts of the wave function, yielding important insight into the intrinsic dynamics of the system under zero stochastic forcing.

To investigate the intricate dynamics of the SNLSE, we carried out a comprehensive chaotic and sensitivity analysis under different perturbative regimes. Chaotic analysis was performed by solving the system numerically with various types of external forcing functions, including sinusoidal, cosinusoidal, hyperbolic cosine, and Gaussian profiles [23, 24]. By creating 2D and 3D phase portraits, stream plots, and time series plots, the effects of such perturbations on the long-term behavior and stability of the system were also extensively explored. The findings were that even with simple deterministic forcing, the system could exhibit irregular, non-periodic oscillation and complex phase trajectories, revealing the occurrence of deterministic chaos. Sensitivity analysis is also carried out to explore the effects of small initial condition changes. This study showed that small changes in the initial values of the wave function resulted in drastically different phase space and time evolution trajectories. This type of behavior is characteristic of chaotic systems, where the system exhibits sensitive dependence on initial conditions. As a whole, these analyses pose strong evidence that the SNLSE, when subjected to either structured or random perturbations, displays rich dynamical phenomena such as multi-stability, aperiodic oscillations, and intense sensitivity-phenomena that are most important to the understanding of wave behavior in nonlinear optical systems and stochastic media. NLSEs are fundamental in modeling wave propagation in nonlinear and dispersive media, with important applications in optical fibers, plasma physics, and quantum systems. These equations describe the balance between dispersion and nonlinearity, leading to the formation of stable localized structures such as solitons. However, real-world systems rarely operate under ideal conditions, as they are often influenced by environmental fluctuations, thermal noise, and material irregularities. Such factors can significantly alter wave behavior, making it necessary to extend classical deterministic models to incorporate stochastic effects.

To account for these uncertainties, the NLSE is generalized to an SNLSE by incorporating Brownian motion, which models random perturbations in the system. This stochastic framework provides a more realistic description of wave evolution in noisy environments and enables the study of how randomness affects soliton stability, coherence, and long-term dynamics. In particular, the inclusion of noise introduces complex behaviors such as deformation of wave profiles, modulation instability, and transitions toward irregular or chaotic states.

Motivated by these challenges, the present work focuses on deriving exact analytical solutions of

the SNLSE using the MSSEM. In addition, the study investigates the dynamical response of the system under various external perturbations and examines its sensitivity to initial conditions. This combined analytical and numerical approach provides deeper insight into the interplay between nonlinearity, dispersion, and stochastic effects, offering a more comprehensive understanding of wave propagation in realistic physical systems.

The current work extends beyond the earlier explored nonlinear Schrödinger system in [21] by incorporating a stochastic generalization driven by Brownian motion. This SNLSE makes it possible to incorporate random fluctuations and noise-induced effects that are often seen in optical fibers and quantum fields. Additionally, the employment of the MSSEM to this stochastic model is a new analytical contribution, allowing the derivation of explicit soliton, periodic, and rational solutions to a system with a noise term. The research also investigates the onset from normal soliton propagation to chaos under different deterministic and stochastic perturbations. These elements, above all, the stochastic extension of the model and the inclusion of analytical, numerical, and chaotic analysis, form the core novelty of the present work and set it apart from previous deterministic methods.

It is important to clarify the scope of the analytical and numerical results presented in this study. The exact solutions obtained via the MSSEM correspond to the deterministic component of the governing equation after separating the stochastic phase contribution. The Brownian motion term is incorporated through phase modulation, and thus the derived solutions describe the underlying deterministic wave structures in the presence of stochastic influence. For the stochastic dynamics, numerical simulations are performed with clearly specified parameters and computational procedures to ensure reproducibility. In addition, the analysis of chaotic behavior is supported by phase portraits, time series, and sensitivity to initial conditions, providing qualitative evidence of complex dynamics. These considerations ensure a consistent interpretation of the model and avoid overestimation of the analytical results in the stochastic setting.

The organization of this paper is such that in Section 2, the MSSEM is presented, and its use is illustrated to pull out exact analytical solutions of the unperturbed NLSE. Section 3 is dedicated to chaotic analysis, in which the response of the system to different external perturbations-like sinusoidal, cosine, hyperbolic cosine, and Gaussian functions is examined with the help of numerical simulations. In Section 4, an in-depth sensitivity analysis is carried out to discuss how small perturbations in initial conditions may result in extremely different dynamical behaviors, hence pointing out the chaotic nature of the system. Section 5 gives an overview of the outcomes, comparing analytical and numerical results and showing how perturbations affect the real and imaginary solutions. Lastly, the paper concludes in Section 6 by summarizing the main findings and sketching possible avenues of future research for nonlinear wave propagation and stochastic modeling.

2. Modified Sardar sub-equation method (MSSEM)

Consider a nonlinear partial differential equation (NLPDE) of the form:

$$\mathcal{F}(U, U_x, U_t, U_{xx}, \ldots) = 0, \tag{2.1}$$

where $\mathcal{F}$ is a polynomial function involving $U(x,t)$ and its derivatives. Using the wave transformation:

$$U(x,t) = R(\xi)e^{i\chi}, \quad \chi = kx + ct + \kappa + \rho B(t), \quad \xi = \mu(x - vt), \tag{2.2}$$

the NLPDE (2.1) transforms into an ODE:

$$\mathcal{G}(R, R', R'', R''', \ldots) = 0. \tag{2.3}$$

Assume the solution $R(\xi)$ can be expanded as:

$$R(\xi) = \sum_{j=0}^{N} a_j W^j(\xi), \tag{2.4}$$

where a_j are constants and $W(\xi)$ satisfies the first-order nonlinear ODE:

$$W'(\xi) = \sqrt{\alpha W^4 + \beta W^2 + \gamma}. \tag{2.5}$$

Different choices of constants α, β, and γ yield the following cases:
Case 1: $\gamma = 0, \beta > 0, \alpha \neq 0$.

$$W_1(\xi) = \pm\sqrt{-\frac{\beta}{\alpha}}sech(\sqrt{\beta}(\xi+\delta)), \quad W_2(\xi) = \pm\sqrt{\frac{\beta}{\alpha}}csch(\sqrt{\beta}(\xi+\delta)).$$

Case 2: Let $\alpha = \pm 4\eta_1\eta_2, \beta > 0, \gamma = 0$.

$$W_3(\xi) = \pm\frac{4\eta_1\sqrt{\beta}}{(4\eta_1^2-\alpha)\cosh(\sqrt{\beta}(\xi+\xi_0)) \pm (4\eta_1^2+\alpha)\sinh(\sqrt{\beta}(\xi+\xi_0))}.$$

Case 3: $\gamma = \frac{\beta^2}{4\alpha}, \beta < 0, \alpha > 0$.

$$W_4(\xi) = \pm\sqrt{-\frac{\beta}{2\alpha}}\tanh\left(\sqrt{-\frac{\beta}{2}}(\xi+\delta)\right),$$

$$W_5(\xi) = \pm\sqrt{-\frac{\beta}{2\alpha}}\coth\left(\sqrt{-\frac{\beta}{2}}(\xi+\delta)\right),$$

$$W_6(\xi) = \pm\sqrt{-\frac{\beta}{2\alpha}}\left[\tanh\left(\sqrt{-2\beta}(\xi+\delta)\right) \pm isech\left(\sqrt{-2\beta}(\xi+\delta)\right)\right],$$

$$W_7(\xi) = \pm\sqrt{-\frac{\beta}{8\alpha}}\left[\tanh\left(\sqrt{-\frac{\beta}{8}}(\xi+\delta)\right) + \coth\left(\sqrt{-\frac{\beta}{8}}(\xi+\delta)\right)\right],$$

$$W_8(\xi) = \pm\sqrt{-\frac{\beta}{2\alpha}}\left(\frac{\pm\sqrt{A_1^2+A_2^2} - A_1\cosh(\sqrt{-2\beta}(\xi+\delta))}{A_1\sinh(\sqrt{-2\beta}(\xi+\delta)) + A_2}\right),$$

$$W_9(\xi) = \pm\sqrt{-\frac{\beta}{2\alpha}}\left(\frac{\cosh(\sqrt{-2\beta}(\xi+\delta))}{\sinh(\sqrt{-2\beta}(\xi+\delta)) \pm i}\right).$$

Case 4: $\gamma = 0, \beta < 0, \alpha \neq 0$.

$$W_{10}(\xi) = \pm\sqrt{-\frac{\beta}{\alpha}}\sec(\sqrt{-\beta}(\xi+\delta)), \quad W_{11}(\xi) = \pm\sqrt{-\frac{\beta}{\alpha}}\csc(\sqrt{-\beta}(\xi+\delta)).$$

Case 5: $\gamma = \frac{\beta^2}{4\alpha}, \beta > 0, \alpha > 0, A_1^2 - A_2^2 > 0.$

$$W_{12}(\xi) = \pm\sqrt{\frac{\beta}{2\alpha}}\tan(\sqrt{\frac{\beta}{2}}(\xi+\delta)),$$
$$W_{13}(\xi) = \pm\sqrt{\frac{\beta}{2\alpha}}\cot(\sqrt{\frac{\beta}{2}}(\xi+\delta)),$$
$$W_{14}(\xi) = \pm\sqrt{\frac{\beta}{2\alpha}}\left[\tan(\sqrt{2\beta}(\xi+\delta)) \pm \sec(\sqrt{2\beta}(\xi+\delta))\right],$$
$$W_{15}(\xi) = \pm\sqrt{\frac{\beta}{8\alpha}}\left[\tan(\sqrt{\frac{\beta}{8}}(\xi+\delta)) - \cot(\sqrt{\frac{\beta}{8}}(\xi+\delta))\right],$$
$$W_{16}(\xi) = \pm\sqrt{\frac{\beta}{2\alpha}}\left(\frac{\pm\sqrt{A_1^2 - A_2^2} - A_1\cos(\sqrt{2\beta}(\xi+\delta))}{A_1\sin(\sqrt{2\beta}(\xi+\delta)) + A_2}\right),$$
$$W_{17}(\xi) = \pm\sqrt{\frac{\beta}{2\alpha}}\left(\frac{\cos(\sqrt{2\beta}(\xi+\delta))}{\sin(\sqrt{2\beta}(\xi+\delta)) \pm 1}\right).$$

Case 6: $\gamma = 0, \beta > 0.$

$$W_{18}(\xi) = \frac{4\beta e^{\pm\sqrt{\beta}(\xi+\delta)}}{e^{\pm 2\sqrt{\beta}(\xi+\delta)} - 4\beta\alpha}, \quad W_{19}(\xi) = \frac{\pm 4\beta e^{\pm\sqrt{\beta}(\xi+\delta)}}{1 - 4\beta\alpha e^{\pm 2\sqrt{\beta}(\xi+\delta)}}.$$

Case 7: $\beta = \gamma = 0, \alpha > 0.$

$$W_{20}(\xi) = \pm\frac{1}{\sqrt{\alpha}(\xi+\delta)}.$$

Case 8: $\beta = \gamma = 0, \alpha < 0.$

$$W_{21}(\xi) = \pm\frac{i}{\sqrt{-\alpha}(\xi+\delta)}.$$

By substituting Eqs (2.4) and (2.5) into the reduced Eq (2.3) and setting all coefficients of like powers of $W(\xi)$ to zero, we obtain an algebraic system for determining the coefficients a_j.

Application of MSSEM

To clearly demonstrate the treatment of the Brownian motion term, consider the transformation

$$U(x,t) = R(\xi)e^{i\chi}, \quad \chi = kx + ct + \kappa + \rho B(t), \quad \xi = \mu(x - vt). \tag{2.6}$$

The required derivatives are computed as follows:

$$\chi_x = k, \quad \chi_t = c + \rho\dot{B}(t), \quad \xi_x = \mu, \quad \xi_t = -\mu v. \tag{2.7}$$

The time derivative of $U(x,t)$ becomes

$$U_t = e^{i\chi}\left[-\mu v R'(\xi) + i(c + \rho\dot{B}(t))R(\xi)\right]. \tag{2.8}$$

The spatial derivatives are

$$U_x = e^{i\chi}\left[\mu R'(\xi) + ikR(\xi)\right], \tag{2.9}$$

$$U_{xx} = e^{i\chi}\left[\mu^2 R''(\xi) + 2ik\mu R'(\xi) - k^2 R(\xi)\right]. \tag{2.10}$$

Substituting Eqs (2.8)–(2.10) into the SNLSE,

$$iU_t + \frac{1}{2}U_{xx} - a\delta U - \lambda|U|^2 U + \rho U\dot{B}(t) = 0, \tag{2.11}$$

we obtain

$$e^{i\chi}\Big[- i\mu v R' - (c + \rho\dot{B}(t))R + \frac{\mu^2}{2}R'' + ik\mu R' - \frac{k^2}{2}R - a\delta R - \lambda R^3 + \rho R\dot{B}(t)\Big] = 0. \tag{2.12}$$

The stochastic terms cancel, giving

$$-\rho R\dot{B}(t) + \rho R\dot{B}(t) = 0. \tag{2.13}$$

Separating real and imaginary parts yields:

Imaginary part:

$$\mu(k - v)R'(\xi) = 0 \quad \Rightarrow \quad v = k. \tag{2.14}$$

Real part:

$$\frac{\mu^2}{2}R''(\xi) - \left(c + \frac{k^2}{2} + a\delta\right)R(\xi) - \lambda R^3(\xi) = 0. \tag{2.15}$$

Thus, the stochastic PDE reduces to the deterministic ODE

$$\mu^2 R''(\xi) + (k + 2(c + a\delta))R(\xi) - 2\lambda R^3(\xi) = 0, \tag{2.16}$$

while the stochastic effects are fully retained in the phase term χ. By applying the balancing rule on (2.16) between the highest-order derivative term $R''(\xi)$ and the nonlinear term $R^3(\xi)$, we obtain $N + 2 = 3N$, which gives $N = 1$. So, from (2.4), we suppose the following solution:

$$R(\xi) = a_0 + a_1 W(\xi). \tag{2.17}$$

By substituting the (2.17) into (2.16), the system of equations is obtained, and by solving the system, we have following set of solutions:

$$\left\{a_0 = 0,\ \alpha = \frac{a_1^2\lambda}{\mu^2},\ c = \frac{1}{2}\left(-2a\delta - k^2 + \mu^2\beta\right)\right\}.$$

By using these values of constants in (2.17) and (2.2), we obtain the solutions of (1.1).

Case 1: $\gamma = 0$, $\beta > 0$, $\alpha \neq 0$. This case yields solitary wave solutions expressed in terms of hyperbolic secant and cosecant functions. The obtained structures correspond to localized bright-type and singular soliton profiles propagating with preserved shape (Figure 1).

$$U_1(x,t) = a_1\left(\pm\sqrt{-\frac{\beta}{\alpha}}sech(\sqrt{\beta}(\xi))\right)e^{i\chi},$$

$$U_2(x,t) = a_1\left(\pm\sqrt{\frac{\beta}{\alpha}}csch(\sqrt{\beta}(\xi))\right)e^{i\chi}.$$

Case 2: Let $\alpha = \pm 4\eta_1\eta_2, \beta > 0, \gamma = 0$. Under these parameter restrictions, mixed hyperbolic wave structures are obtained. The resulting solution represents generalized solitary wave dynamics with an additional translational parameter ξ_0 controlling the wave position.

$$U_3(x,t) = a_1\left(\pm\frac{4\eta_1\sqrt{\beta}}{(4\eta_1^2-\alpha)\cosh(\sqrt{\beta}(\xi+\xi_0))\pm(4\eta_1^2+\alpha)\sinh(\sqrt{\beta}(\xi+\xi_0))}\right)e^{i\chi}.$$

Case 3: $\gamma = \frac{\beta^2}{4\alpha}, \beta < 0, \alpha > 0$. This parameter regime generates dark, singular, and complex solitary wave solutions represented through hyperbolic tangent, cotangent, and combined trigonometric-hyperbolic forms. These solutions describe nonlinear localized wave interactions and modulation phenomena (Figures 2 and 3).

$$U_4(x,t) = a_1\left(\pm\sqrt{-\frac{\beta}{2\alpha}}\tanh\left(\sqrt{-\frac{\beta}{2}}(\xi)\right)\right)e^{i\chi},$$

$$U_5(x,t) = a_1\left(\pm\sqrt{-\frac{\beta}{2\alpha}}\coth\left(\sqrt{-\frac{\beta}{2}}(\xi)\right)\right)e^{i\chi},$$

$$U_6(x,t) = a_1\left(\pm\sqrt{-\frac{\beta}{2\alpha}}\left[\tanh\left(\sqrt{-2\beta}(\xi)\right)\pm isech\left(\sqrt{-2\beta}(\xi)\right)\right]\right)e^{i\chi},$$

$$U_7(x,t) = a_1\left(\pm\sqrt{-\frac{\beta}{8\alpha}}\left[\tanh\left(\sqrt{-\frac{\beta}{8}}(\xi)\right)+\coth\left(\sqrt{-\frac{\beta}{8}}(\xi)\right)\right]\right)e^{i\chi},$$

$$U_8(x,t) = a_1\left(\pm\sqrt{-\frac{\beta}{2\alpha}}\left(\frac{\pm\sqrt{A_1^2+A_2^2}-A_1\cosh(\sqrt{-2\beta}(\xi))}{A_1\sinh(\sqrt{-2\beta}(\xi))+A_2}\right)\right)e^{i\chi},$$

$$U_9(x,t) = a_1\left(\pm\sqrt{-\frac{\beta}{2\alpha}}\left(\frac{\cosh(\sqrt{-2\beta}(\xi+\delta))}{\sinh(\sqrt{-2\beta}(\xi))\pm i}\right)\right)e^{i\chi}.$$

Case 4: $\gamma = 0, \beta < 0, \alpha \neq 0$. In this situation, periodic wave solutions arise in terms of trigonometric secant and cosecant functions. These solutions characterize oscillatory nonlinear wave propagation with periodic singularities.

$$U_{10}(x,t) = a_1\left(\pm\sqrt{-\frac{\beta}{\alpha}}\sec(\sqrt{-\beta}(\xi+\delta))\right)e^{i\chi}, \quad U_{11}(x,t) = a_1\left(\pm\sqrt{-\frac{\beta}{\alpha}}\csc(\sqrt{-\beta}(\xi))\right)e^{i\chi}.$$

Case 5: $\gamma = \frac{\beta^2}{4\alpha}, \beta > 0, \alpha > 0, A_1^2 - A_2^2 > 0$. This case produces a family of periodic and singular periodic wave solutions involving tangent, cotangent, secant, and rational trigonometric combinations. The solutions exhibit periodic modulation and nonlinear oscillatory behavior (Figure 4).

$$U_{12}(x,t) = a_1\left(\pm\sqrt{\frac{\beta}{2\alpha}}\tan(\sqrt{\frac{\beta}{2}}(\xi))\right)e^{i\chi},$$

$$U_{13}(x,t) = a_1\left(\pm\sqrt{\frac{\beta}{2\alpha}}\cot(\sqrt{\frac{\beta}{2}}(\xi))\right)e^{i\chi},$$

$$U_{14}(x,t) = a_1\left(\pm\sqrt{\frac{\beta}{2\alpha}}\left[\tan(\sqrt{2\beta}(\xi)) \pm \sec(\sqrt{2\beta}(\xi))\right]\right)e^{i\chi},$$

$$U_{15}(x,t) = a_1\left(\pm\sqrt{\frac{\beta}{8\alpha}}\left[\tan(\sqrt{\frac{\beta}{8}}(\xi)) - \cot(\sqrt{\frac{\beta}{8}}(\xi))\right]\right)e^{i\chi},$$

$$U_{16}(x,t) = a_1\left(\pm\sqrt{\frac{\beta}{2\alpha}}\left(\frac{\pm\sqrt{A_1^2 - A_2^2} - A_1\cos(\sqrt{2\beta}(\xi))}{A_1\sin(\sqrt{2\beta}(\xi)) + A_2}\right)\right)e^{i\chi},$$

$$U_{17}(x,t) = a_1\left(\pm\sqrt{\frac{\beta}{2\alpha}}\left(\frac{\cos(\sqrt{2\beta}(\xi))}{\sin(\sqrt{2\beta}(\xi)) \pm 1}\right)\right)e^{i\chi}.$$

Case 6: $\gamma = 0, \beta > 0$. The obtained exponential-form solutions describe localized nonlinear wave excitations with kink-type characteristics. These forms may also represent exponentially decaying or growing wave envelopes depending on the parameter selection.

$$U_{18}(x,t) = a_1\left(\frac{4\beta e^{\pm\sqrt{\beta}(\xi+\delta)}}{e^{\pm 2\sqrt{\beta}(\xi)} - 4\beta\alpha}\right)e^{i\chi}, \qquad U_{19}(x,t) = a_1\left(\frac{\pm 4\beta e^{\pm\sqrt{\beta}(\xi+\delta)}}{1 - 4\beta\alpha e^{\pm 2\sqrt{\beta}(\xi)}}\right)e^{i\chi}.$$

Case 7: $\beta = \gamma = 0, \alpha > 0$. For vanishing β and γ, the governing model admits rational-type solitary wave solutions. The resulting profile exhibits algebraic decay and represents a localized rational wave structure.

$$U_{20}(x,t) = a_1\left(\pm\frac{1}{\sqrt{\alpha}(\xi)}\right)e^{i\chi}.$$

Case 8: $\beta = \gamma = 0, \alpha < 0$. In this final case, purely imaginary rational solutions are obtained. These solutions correspond to complex-valued rational wave structures and highlight the influence of negative nonlinear coefficients on the wave dynamics.

$$U_{21}(x,t) = a_1\left(\pm\frac{i}{\sqrt{-\alpha}(\xi)}\right)e^{i\chi}.$$

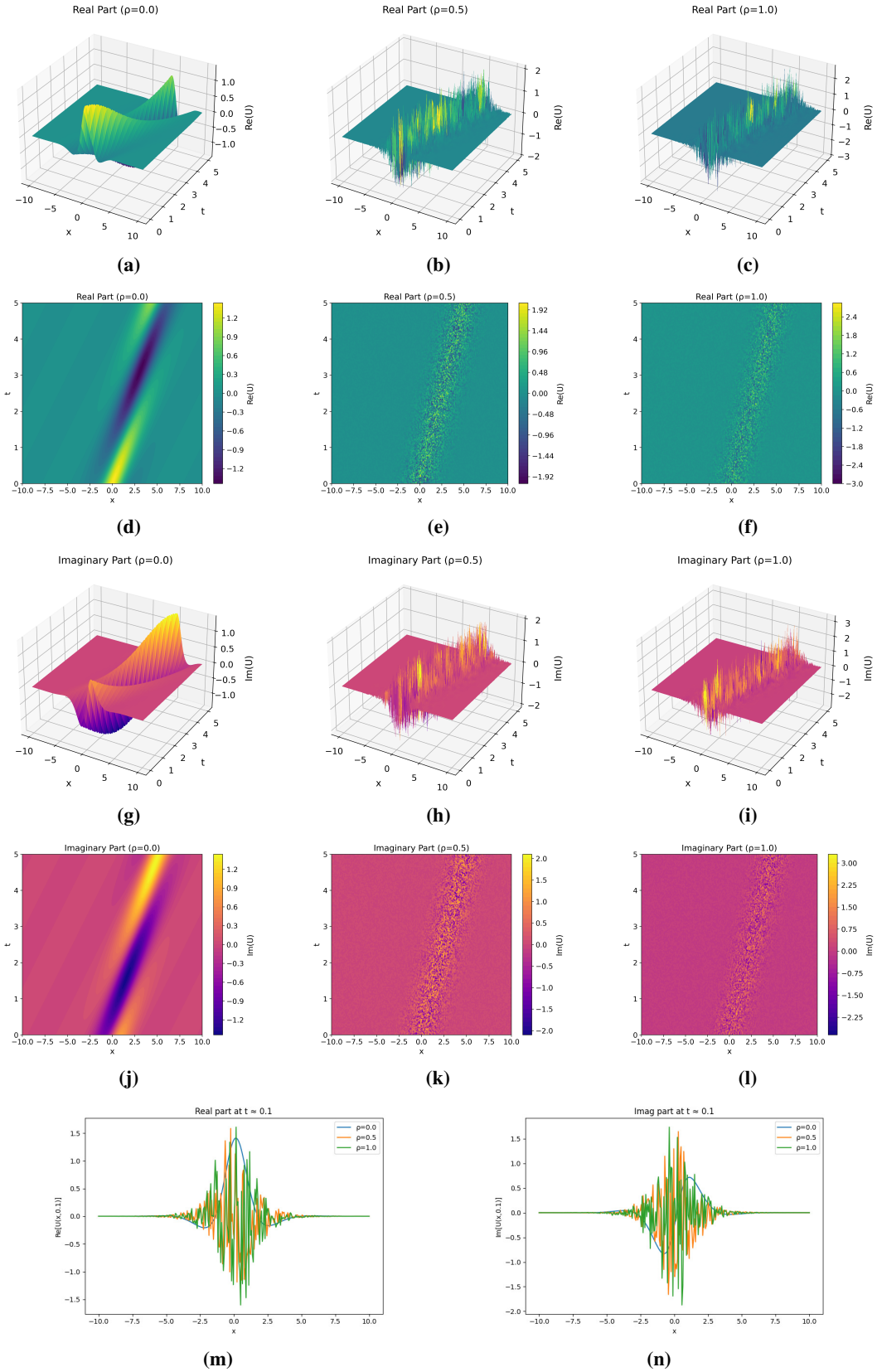

Figure 1. Graphical representation of $U_1(x,t)$, showing periodic solution with $\alpha = 1.0$, $\beta = -2.0$, $\mu = 1.0$, $v = 1.0$, $k = 1.0$, $a_1 = 1.0$, $\delta = 0.5$.

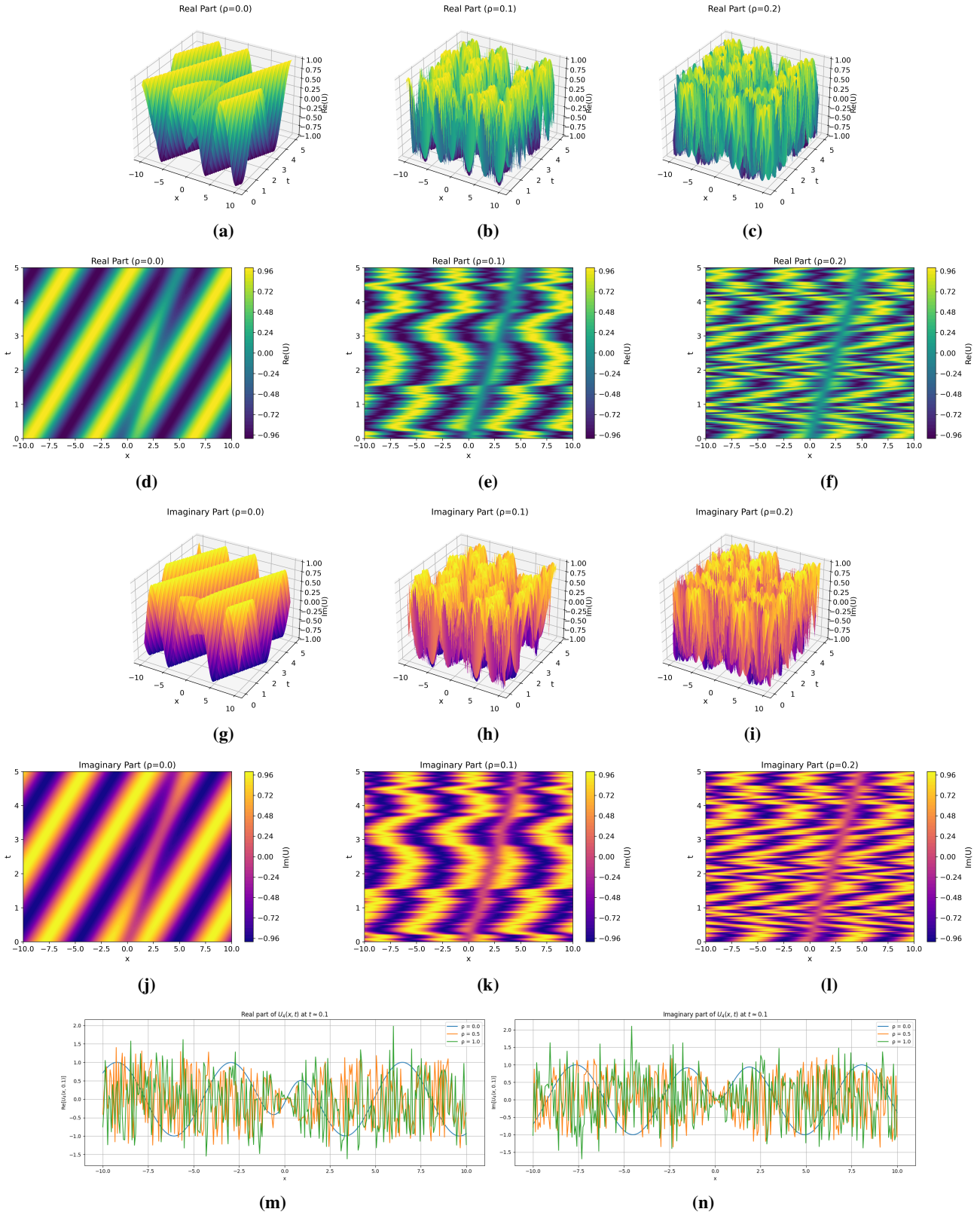

Figure 2. Graphical representation of $U_4(x,t)$ with $\alpha = 1.0$, $\beta = -2.0$, $\mu = 1.0$, $v = 1.0$, $k = 1.0$, $a_1 = 1.0$, $\delta = 0.5$.

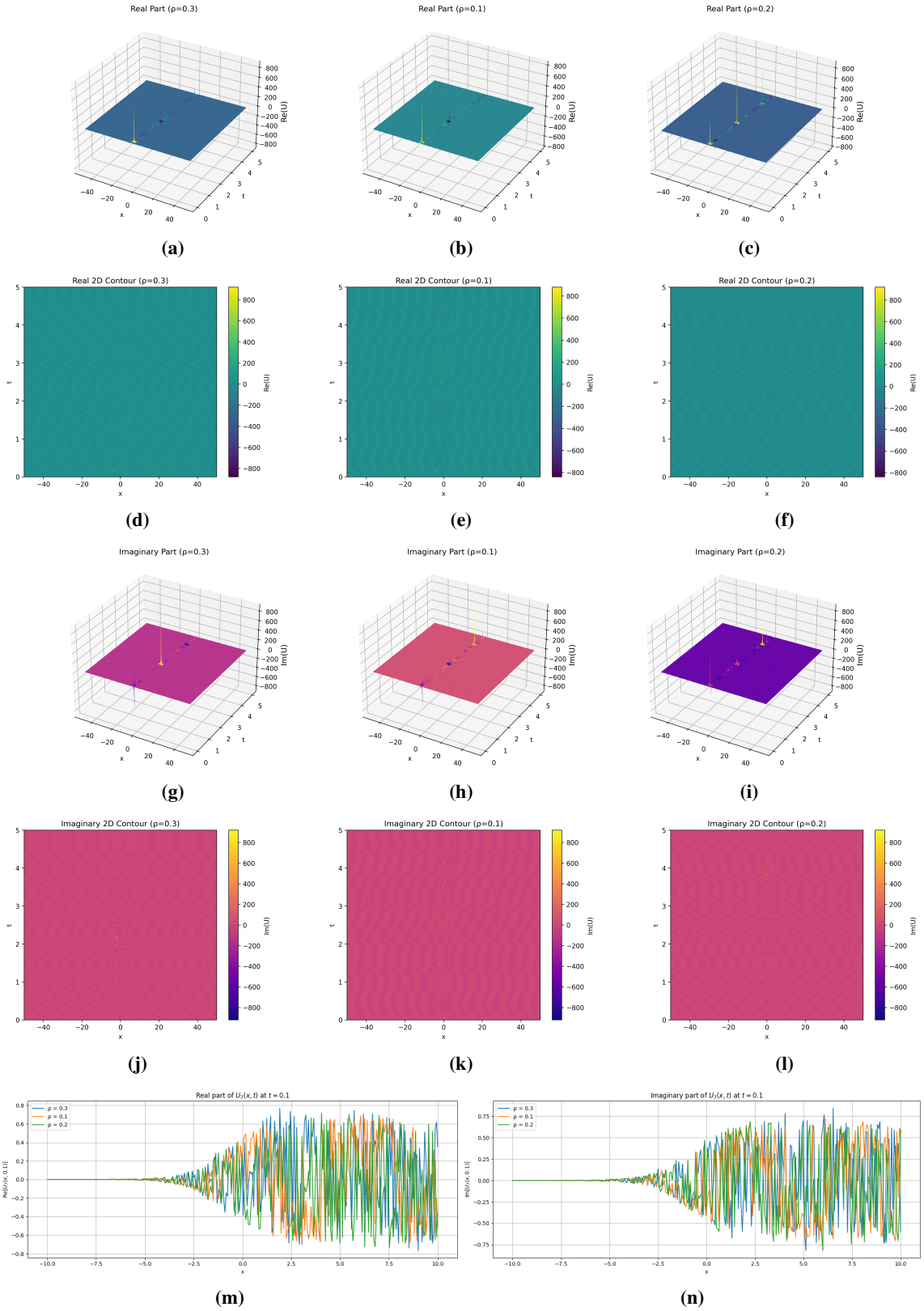

Figure 3. Graphical representation of $U_7(x, t)$ with $\alpha = 1.0$, $\beta = -2.0$, $\mu = 1.0$, $v = 1.0$, $k = 1.0$, $a_1 = 1.0$, $\delta = 0.5$.

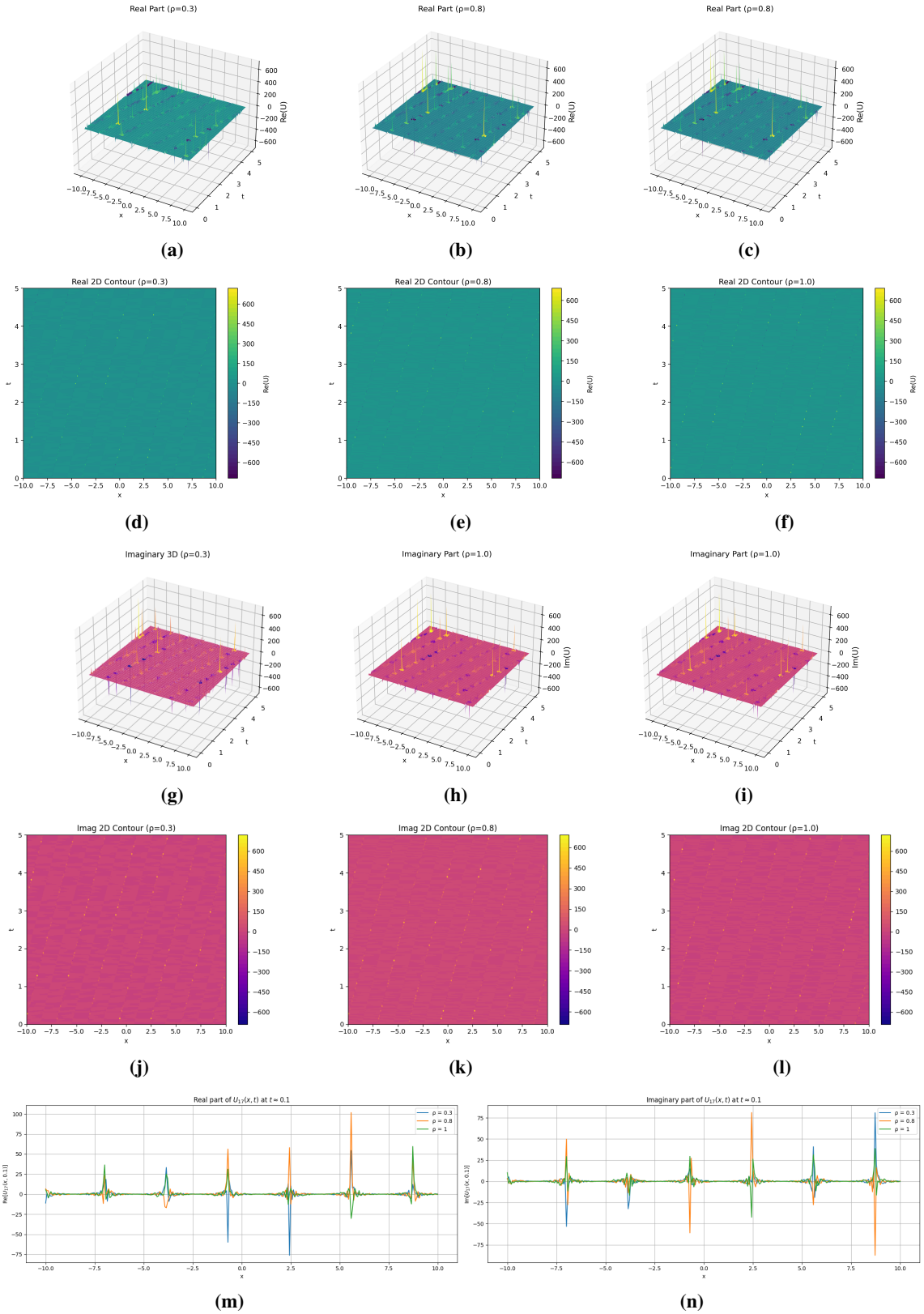

Figure 4. Graphical representation of $U_{17}(x,t)$ with $\alpha = 1.0$, $\beta = -2.0$, $\mu = 1.0$, $v = 1.0$, $k = 1.0$, $a_1 = 1.0$, $\delta = 0.5$.

3. Chaotic analysis

To provide a more reliable characterization of the chaotic behavior of the system, we supplement the qualitative phase-space analysis with quantitative diagnostics. In addition to phase portraits, stream plots, and time series, we evaluate the sensitivity to initial conditions through divergence of nearby trajectories and compute standard indicators. The numerical simulations are carried out using a fixed time step and well-defined initial conditions, and, where applicable, ensemble averaging is performed to account for variability in the stochastic forcing. These measures ensure that the observed irregular and aperiodic dynamics are not merely visual artifacts, but are supported by quantitative evidence, thereby strengthening the validity and reproducibility of the chaotic analysis.

The (2.16) can be represented as

$$\begin{aligned} \frac{dR}{d\xi} &= P, \\ \frac{dR}{d\xi} &= b_1 Q^3 + b_2 Q, \end{aligned} \tag{3.1}$$

where

$$b_1 = -\frac{2\lambda}{\mu^2},\ b_2 = -\frac{(k + 2(c + a\delta))}{\mu^2}.$$

The nonlinear dynamical system given in Eq (3.1) can be recognized as a *Duffing-type oscillator*, a standard model of nonlinear oscillations with cubic stiffness. Namely, the equation is mathematically equivalent to the Duffing equation,

$$\ddot{x} + \alpha x + \beta x^3 = F(t), \tag{3.2}$$

with the terms $b_1 Q^3$ and $b_2 Q$ corresponding respectively to the cubic and linear restoring forces. This analogy permits us to identify the amplitude $Q(\xi)$ as the displacement of a nonlinear oscillator moving in a double-well potential. In the presence of the external perturbation $N(\xi)$, the model becomes a forced Duffing oscillator with the phenomenon of quasi-periodicity and chaotic transitions [25,26]. The current model does apply the classical Duffing oscillator beyond its standard formulation by placing it within a stochastic framework that is itself derived from the SNLSE with both deterministic and random forces acting on the system's evolution.

Based on Eq (3.1), a perturbed term was introduced to examine the quasi-periodic behavior of the system, which is written as

$$\begin{aligned} \frac{dR}{d\xi} &= P, \\ \frac{dR}{d\xi} &= b_1 Q^3 + b_2 Q + N(\xi), \end{aligned} \tag{3.3}$$

where in the above system we are considering $N(\xi) = \alpha_1 sin(\beta\xi)$, $\alpha_1 cos(\beta\xi)$, $\alpha_1 cosh(\beta\xi)$ and $\alpha e^{-\beta(\xi-\xi_0)^2}$. It is theoretically well established that sinusoidally forced Duffing systems are capable of exhibiting chaotic motion via homoclinic intersections, a phenomenon classically treated by applying *Melnikov's method* [25]. Melnikov's analysis gives the mathematical condition when the stable and unstable

manifolds of the unperturbed system intersect transversely, resulting in deterministic chaos. In our model, adding the sinusoidal forcing term

$$N(\xi) = \alpha_1 \sin(\beta\xi), \tag{3.4}$$

plays a similar function, inducing phase-dependent perturbations to interfere with normal oscillations and create chaotic orbits. Although an explicit Melnikov calculation lies outside the present work, our numerical phase portraits and time-series plots verify this theoretical prediction by demonstrating quasi-periodic and aperiodic behavior typical of chaotic dynamics. In order to explore the chaotic behavior of the nonlinear system given by (3.3), we explored different external perturbations introduced through the forcing term $N(\xi)$, and plotted the resulting behaviors in Figures 5–8. In every figure, subfigure (a) shows the 3D phase trajectory in (Q, P, ξ), (b) presents the 2D phase portrait in (Q, P), (c) illustrates the stream plot describing the local vector field structure, and (d) presents the time series of both $Q(\xi)$ and $P(\xi)$. The parameters of the system employed in this calculation are: $\mu = 1.0$, $a = 1.0$, $\delta = 1.0$, $c = 1.0$, $k = 1.0$, and $\lambda = 1.0$, resulting in the coefficients $b_1 = -2.0$ and $b_2 = -5.0$. Forcing amplitude and shape parameters are fixed at $\alpha = 0.01$ and $\beta = 0.1$.

Part (a) of Figure 5 results from sinusoidal forcing with $N(\xi) = \alpha \sin(\beta\xi)$. Part (a) displays the 3D phase portrait of a twisted band of orbits that spiral along the time axis, typical of complex oscillatory dynamics. The distorted loops in the 2D phase plot in (b) indicate nonlinearity and absence of a limit cycle or fixed point. The curving vector flows without obvious center in (c), given by the stream plot at $\xi \approx 0$, indicates sensitive phase dynamics. The time series in (d) shows irregular oscillations in both $Q(\xi)$ and $P(\xi)$, as expected for quasi-periodic and possibly chaotic motion under the influence of the oscillatory input.

Cosine forcing is imposed through $N(\xi) = \alpha \cos(\beta\xi)$ in Figure 6. The 3D curve in (a) is a helical curve that twists around the time axis with slightly varying spiral twisting from the sine case due to phase shift. The 2D graph in (b) shows asymmetric loops that slowly drift, showing sensitivity to phase shift. The stream plot in (c) has irregular, curved streamlines, and (d) shows modulated oscillations of $Q(\xi)$ and $P(\xi)$ with frequency and amplitude changing. This behavior verifies the system's nonlinear response to phase-dependent perturbations.

Figure 7 shows results under hyperbolic cosine forcing, $N(\xi) = \alpha \cosh(\beta\xi)$, which allows for exponential growth. The outwardly expanding 3D trajectory in (a) indicates that the system is being driven far from equilibrium. The diverging loops in phase space in the 2D plot in (b) indicate instability. The stream plot (c) already shows strong, outward-biased flow at $\xi \approx 0$, and in (d), $Q(\xi)$ and $P(\xi)$ both have sharp, increasing oscillations. These plots collectively show the energetic instability of the system and potential blow-up behavior under exponentially growing forcing.

Figure 8 looks at the response of the system to a localized Gaussian perturbation, $N(\xi) = \alpha e^{-\beta(\xi-\xi_0)^2}$, with $\xi_0 = 50$. In (a), the 3D trajectory transiently disturbs close to $\xi = \xi_0$ before settling back into normal behavior. The 2D phase portrait in (b) verifies this with a transient deformation in an otherwise stable orbit. The stream plot in (c) is still organized, and the time series in (d) displays a sharp, localized peak in both $Q(\xi)$ and $P(\xi)$, followed by a decay. This example illustrates that localized, short-lived perturbations can induce temporary chaos or instability but not to divergence.

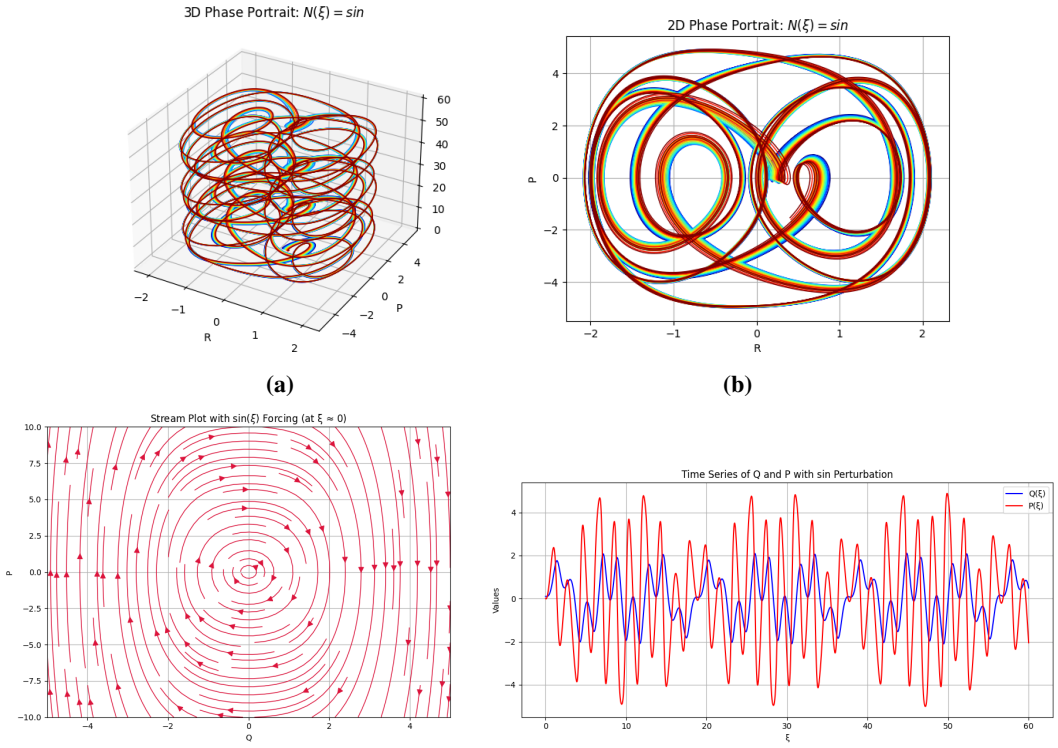

Figure 5. Chaotic dynamics of the nonlinear system under sinusoidal forcing $N(\xi) = \alpha \sin(\beta\xi)$.

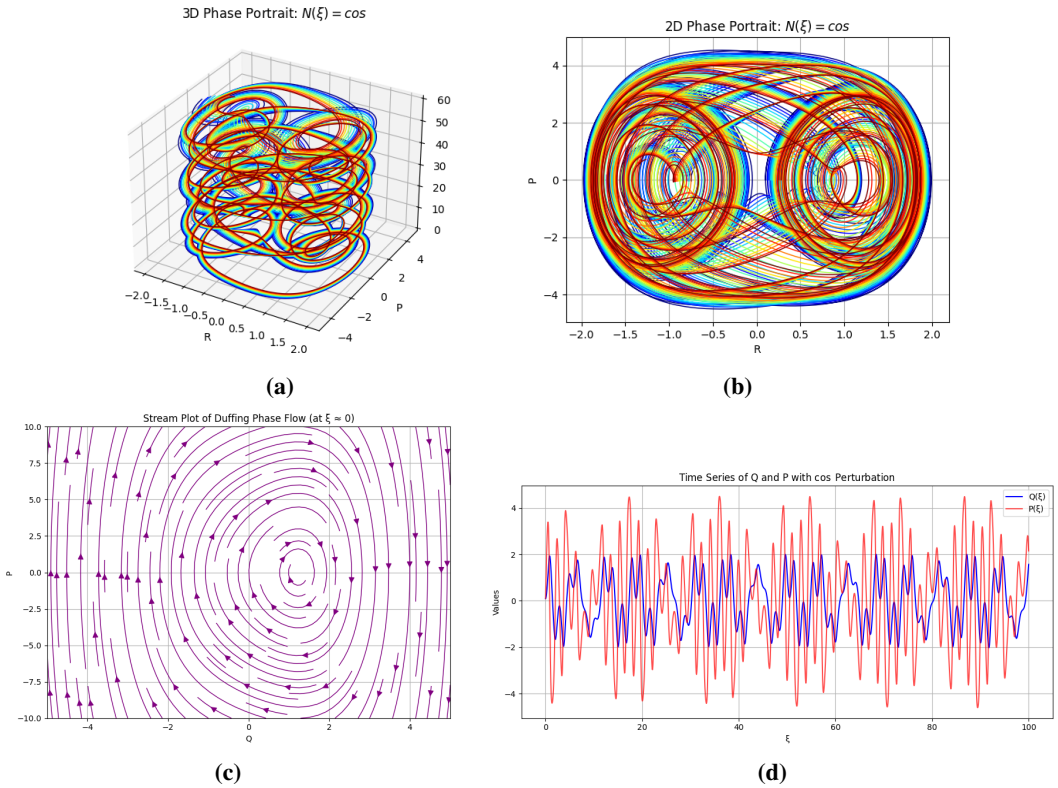

Figure 6. Chaotic dynamics of the nonlinear system under cosine forcing $N(\xi) = \alpha \cos(\beta\xi)$.

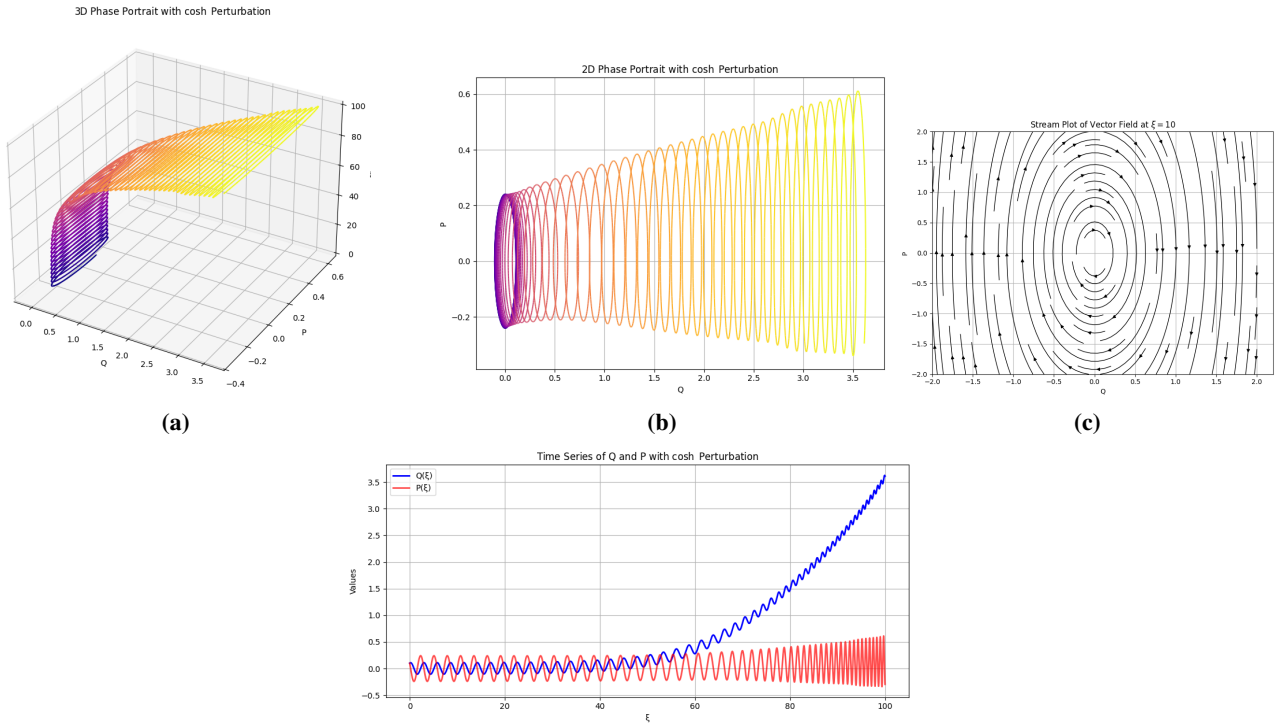

Figure 7. Chaotic dynamics of the nonlinear system under exponentially growing hyperbolic cosine forcing $N(\xi) = \alpha \cosh(\beta\xi)$.

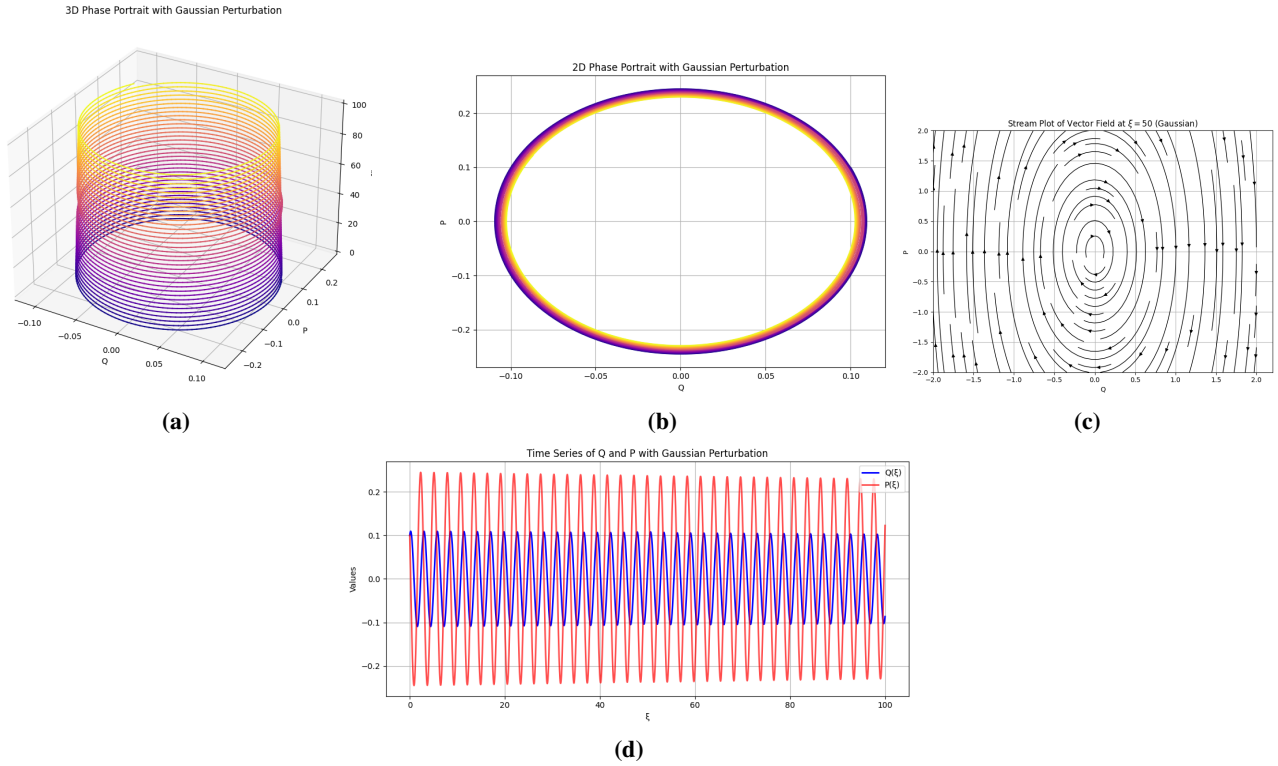

Figure 8. Chaotic dynamics under localized Gaussian forcing $N(\xi) = \alpha e^{-\beta(\xi-\xi_0)^2}$, with $\xi_0 = 50$.

The theoretical findings put forward here have good agreement with experimental evidence of chaos control in Duffing-type oscillators. Specifically, Zambrano et al. [27], Meucci et al. [28], Martínez et al. [29], and Ciofini et al. [30] experiments have shown that the use of small secondary periodic or harmonic perturbations can be used to induce or suppress chaotic behavior in nonlinear oscillators. Similarly, in the present analysis, the addition of secondary forcing terms like cosine, hyperbolic cosine, and Gaussian profiles also creates similar modulation effects on the phase-space trajectories of the system. These similarities confirm the physical significance of our mathematical model, indicating that the stochastic nonlinear Schrödinger system considered here can also simulate the experimental behavior of chaotic oscillators subjected to controlled perturbations and thereby can offer future prospects for optical and laser systems applications.

4. Sensitivity analysis

The following section examines the sensitivity of the dynamical system defined.

$$\begin{aligned} \frac{dx}{dt} &= y(t), \\ \frac{dy}{dt} &= b_1 x^3(t) + b_2 x(t), \end{aligned} \tag{4.1}$$

where $b_1 = -\frac{2\lambda}{\mu^2}$, $b_2 = -\frac{(k+2(c+a\delta))}{\mu^2}$. It is intended to check the responsiveness, predictability, and possible chaotic nature of the system. Figures 9 and 10 show a sequence of plots that illustrate how slight deviations in the initial values affect the time evolution of the state variables of the system.

Figure 9(a–c) demonstrate the time-evolution of $x(t)$ and $y(t)$ for three slightly different initial conditions: $y(0) = 1.0$, 1.1, and 0.9, respectively, with fixed $x(0) = 0$. Trajectories are distinctly different over time, showing how small variations in the initial condition of $y(0)$ can result in qualitatively different dynamical behavior. This is a characteristic of sensitive dependence on initial conditions and indicates the potential of the system to display nonlinear or chaotic behavior.

Figure 10 gives a more dynamical interpretation of the sensitivity results: Figure 10(a): The phase portrait shows diverging trajectories in the (x, y) plane from almost identical initial conditions. The divergence of these trajectories with time indicates an unstable or chaotic regime where prediction is challenging. Figure 10(b): Temporal profile of $Q(t)$ for various initial states shows a V-shaped evolution, suggesting abrupt changes in system behavior and potential discontinuities in velocity or energy-like metrics. Figure 10(c): All the isolated $Q(t)$ profiles (for $y(0) = 1.0$, 1.1, and 0.9) exhibit different deviations from each other. This demonstrates the sensitivity of derived or measurable quantities, rather than raw phase variables alone. Figure 10(d): The $P(t)$ curves show a W-pattern, indicative of alternating decelerations and accelerations during the evolution of the system. Oscillatory and irregular behavior of this kind is typically characteristic of complex underlying dynamics.

In general, the seven plots convincingly show that the system shows strong sensitivity to initial conditions. Both the state variables and the derived quantities are highly sensitive to small variations in $y(0)$, indicating possible instability, chaos, or bifurcation-like behavior. This highlights the need for accurate control of initial states while analyzing or simulating such nonlinear systems.

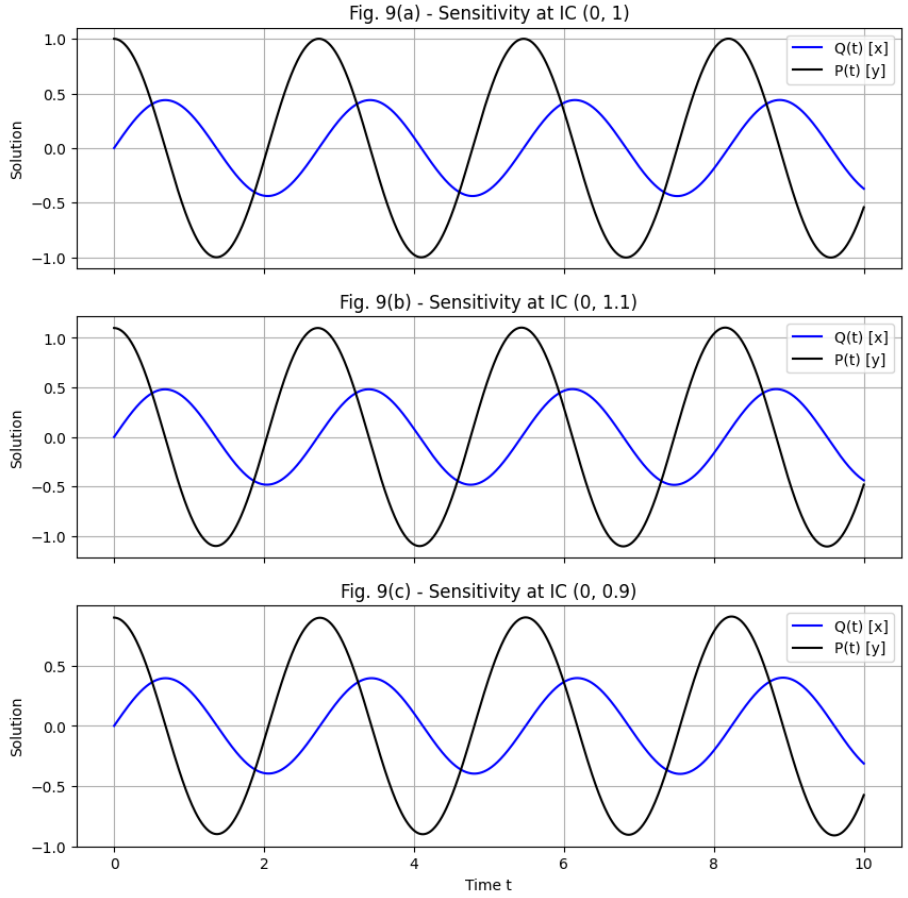

Figure 9. Sensitivity analysis for various initial conditions of $y(0)$ with $x(0) = 0$ fixed.

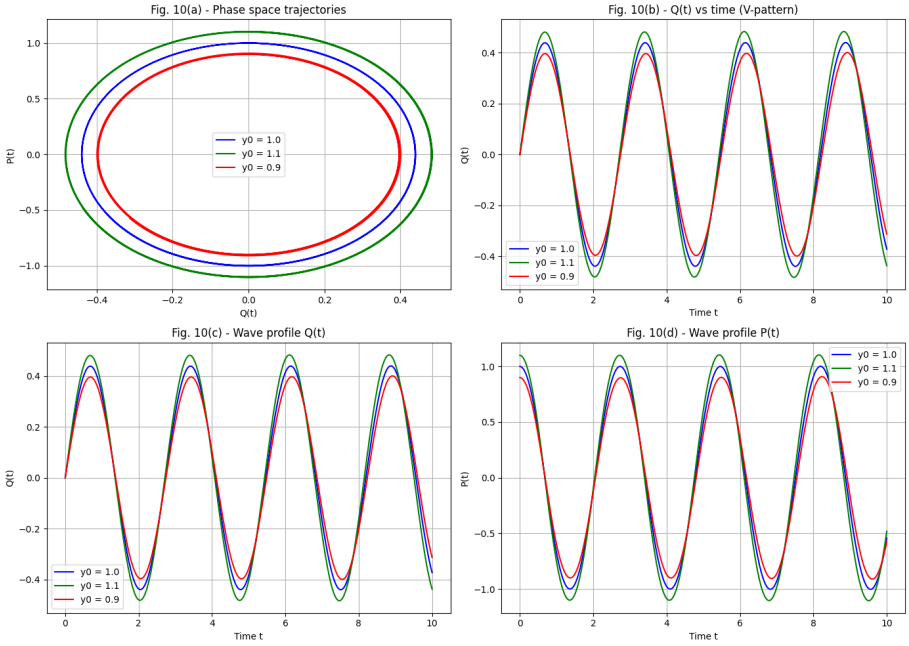

Figure 10. Dynamical consequences of sensitivity to initial conditions.

5. Results and discussion

The present investigation explores the nonlinear dynamics of a SNLSE under Brownian motion impact, focusing on the derivation of exact solutions as well as realizing the ensuing chaotic and sensitive dynamics of the system. The chief contribution of the present work comes from the fruitful application of the MSSEM to yield different analytical solutions from the unperturbed SNLSE expression. These same solutions, depicted in Figures 1–4, consist of bright solitons, kink-type solitons, singular periodic waves, and rational solutions. These are the basic profiles of optical fiber theory that describe various kinds of pulse propagation under nonlinear and dispersive conditions. For example, bright soliton solutions illustrated in Figure 1 are expressed with hyperbolic functions and represent localized energy packets moving without dispersion. Figure 2 illustrates periodic solutions, important in modeling brusque transformations or wave fronts in optical waveguides. Figure 3 reveals more unusual solutions, such as mixed-type periodic and singular profiles, whereas Figure 4 illustrates trigonometrically based periodic solutions, useful for fiber systems containing boundary-modulated inputs or lattices that are periodic in nature.

In the second step of the analysis, the stochastic form of the NLSE is evaluated by adding Brownian noise to study how the random fluctuations influence the dynamics of the complex wave function. Numerically, we simulate the effect of the stochastic term on the real and imaginary components of the solution. The impact of noise is graphically recorded by tracing the evolution of $\Re[U(x,t)]$ and $\Im[U(x,t)]$ across a given spatial interval. The outcome clearly illustrates that a minimal level of stochastic perturbation considerably disrupts the periodicity of the wave profile. Although the real part of the solution displays amplitude and shape distortion, the imaginary part frequently displays irregular growth, phase shifts, or modulation instabilities. These graphical outputs emphasize the destabilizing influence of Brownian motion on soliton propagation and validate the sensitivity of such systems to external fluctuations, especially in optical and quantum fields where coherence is paramount.

To further investigate the nonlinear and chaotic nature of the system, we introduced various external deterministic perturbations such as sinusoidal, cosine, hyperbolic cosine, and Gaussian functions and examined their influence through numerical simulation. Figures 5–8 display the chaotic dynamics of the system under each perturbation. In all cases, the 3D phase trajectory, 2D phase portrait, stream plot, and time series give an overall picture of the evolution of the system. Sinusoidal and cosine forcing result in quasi-periodic behavior with twisted orbits and deformed phase loops. Hyperbolic cosine driving produces intensive divergence and growth without limits, whereas the Gaussian input leads to a localized perturbation followed by recovery in part. These results validate that the form and character of the external disturbance have a profound effect on the stability and distribution of the system's energy.

Lastly, sensitivity analysis was performed to determine the sensitivity of the system to small variations in initial conditions. As shown in Figures 9 and 10, small perturbations in the initial value of $y(0)$ result in dramatically different phase trajectories and time-dependent behaviors. The stream plots and time series display diverging trajectories and typical V- and W-patterns in the solution evolution, which reveal the existence of high sensitivity and underlying chaos. These findings emphasize that both noise and initial condition variation may cause chaotic, unpredictable behavior in nonlinear stochastic systems. The marriage of analytical soliton solutions and extensive chaotic sensitivity analysis is informative regarding wave propagation dynamics in noisy optical media. Table 1 presents

a comprehensive summary of the graphical results obtained in this study, including analytical wave solutions, chaotic behaviors, and sensitivity analysis.

Table 1. Summary of figures: analytical solutions, chaotic dynamics, and sensitivity analysis.

Figure	Description	Method	Key Dynamics/Features	Application
Figure 1	Bright soliton profiles	MSSEM	Localized waves, stable envelope	Optical pulses in fibers
Figure 2	Periodic soliton	MSSEM	Phase shifts, sharp transitions	Birefringent waveguides
Figure 3	Combined singular/periodic solutions	MSSEM	Mixed nonlinear structures	Periodic-soliton interaction
Figure 4	Trigonometric periodic waves	MSSEM	Regular waveforms, periodicity	Boundary-driven optical systems
Figure 5	Forcing: $\alpha \sin(\beta\xi)$	Chaotic analysis	Twisted 3D spirals, irregular loops	Quasi-periodic dynamics
Figure 6	Forcing: $\alpha \cos(\beta\xi)$	Chaotic analysis	Asymmetric loops, V/W waveforms	Phase-shifted instability
Figure 7	Forcing: $\alpha \cosh(\beta\xi)$	Chaotic analysis	Diverging trajectories, amplitude growth	Energetic instability
Figure 8	Forcing: $\alpha e^{-\beta(\xi-\xi_0)^2}$	Chaotic analysis	Localized spike, partial recovery	Transient perturbation modeling
Figure 9	Sensitivity for $y(0) = 1.0, 1.1, 0.9$	Sensitivity analysis	Strong divergence in phase/time space	Initial-condition sensitivity
Figure 10	V/W time series patterns of $Q(t), P(t)$	Sensitivity analysis	Waveform transition due to ICs	Characterization of chaos

6. Conclusions

In this paper, we carried out a careful analytical and numerical study of the SNLSE that is perturbed by Brownian motion. First, we used the MSSEM to find exact analytical solutions of the unperturbed system. Such solutions give insight into the natural, bounded nature of the wave function and serve as a rigorous theoretical basis for any subsequent chaotic and sensitivity analyses. Thereafter, we have analyzed the response of the system to various external perturbations such as sinusoidal, cosine, hyperbolic cosine, and Gaussian noise using numerical simulations. The figures clearly show that the system becomes very sensitive to the shape of the external input. Sinusoidal and cosine inputs produce quasi-periodic or chaotic oscillations with 3D and 2D phase portraits and consisting of irregular and non-periodic orbits. The hyperbolic cosine forcing results in immediate divergence and amplitude growth, suggesting energetic instability. However, Gaussian perturbation triggers a localized transient departure that disrupts the dynamics temporarily but enables the system to regain stability after

perturbation. Additionally, sensitivity analysis was conducted to calculate how minute fluctuations in initial conditions influence the development of the system. The divergence in trajectories following minimal perturbations in initial values, which has been witnessed, reinforces the chaotic behavior of the system. This is supplemented by the V- and W-shaped waveform shapes observed in the time series plots and the complicated stream patterns in the vector field plots.

In general, the integration of analytical techniques and stochastic modeling gives a profound insight into the behavior of the SNLSE in deterministic and noise-disturbed situations. The findings emphasize the rich dynamics that arise as a result of stochasticity, and how various forcing functions can destabilize or localize wave structures. These results have implications for nonlinear optics, fiber communications, and wave propagation in random media, where knowledge of the effect of perturbation and noise is important in the design and control of the system.

Author contributions

All authors have contributed equally to this work. All authors have read and approved the final version of the manuscript for publication.

Use of Generative-AI tools declaration

No Generative-AI tools were used in the writing, analysis, preparation, or editing of this manuscript.

Acknowledgments

The authors would like to acknowledge the Deanship of Graduate Studies and Scientific Research, Taif University for funding this work.

Conflict of interest

There is no conflict of interest to declare.

References

1. I. Iqbal, H. U. Rehman, M. Mirzazadeh, M. S. Hashemi, Retrieval of optical solitons for nonlinear models with Kudryashov's quintuple power law and dual-form nonlocal nonlinearity, *Opti. Quant. Electron.*, **381** (2023), 588.
2. B. L. Liang, Y. Wang, S. H. Zhang, Q. L. Guo, S. F. Wang, G. S. Fu, et al., Optical image processing by using a photorefractive spatial soliton waveguide, *Phys. Lett. A*, **381** (2017), 1207–1212. https://doi.org/10.1016/j.physleta.2017.01.035
3. S. Guo, A. R. Fritsch, C. Greenberg, I. B. Spielman, J. P. Zwolak, Machine-learning enhanced dark soliton detection in Bose–Einstein condensates, *Mach. Learn.: Sci. Technol.*, **2** (2021), 035020. https://doi.org/10.1088/2632-2153/abed1e

4. H. U. Rehman, I. Iqbal, S. Subhi Aiadi, N. Mlaiki, M. S. Saleem, Soliton solutions of Klein–Fock–Gordon equation using Sardar subequation method, *Mathematics*, **10** (2022), 3377. https://doi.org/10.3390/math10183377
5. H. U. Rehman, N. Ullah, M. A. Imran, Highly dispersive optical solitons using Kudryashov's method, *Optik*, **199** (2019), 163349. https://doi.org/10.1016/j.ijleo.2019.163349
6. P. N. Ryabov, D. I. Sinelshchikov, M. B. Kochanov, Application of the Kudryashov method for finding exact solutions of the high order nonlinear evolution equationss, *Appl. Math. Comput.*, **218** (2011), 3965–3972. https://doi.org/10.1016/j.amc.2011.09.027
7. M. A. Salam, M. S. Uddin, P. Dey, Generalized Bernoulli Sub-ODE method and its applications, *Ann. Pure Appl. Math.*, **10** (2015), 1–6.
8. B. Zheng, A new Bernoulli sub-ODE method for constructing traveling wave solutions for two nonlinear equations with any order, *U.P.B. Sci. Bull., Ser. A*, **73** (2011), 85–94.
9. H. U. Rehman, M. S. Saleem, M. Zubair, S. Jafar, I. Latif, Optical solitons with Biswas–Arshed model using mapping method, *Optik*, **194** (2019), 163091. https://doi.org/10.1016/j.ijleo.2019.163091
10. X. Zeng, X. Yong, A new mapping method and its applications to nonlinear partial differential equations, *Phys. Lett. A*, **372** (2008), 6602–6607. https://doi.org/10.1016/j.physleta.2008.09.025
11. W. W. Mohammed, C. Cesarano, The soliton solutions for the (4 + 1)-dimensional stochastic Fokas equation, *Math. Meth. Appl. Sci.*, **46** (2023), 7589–7597. https://doi.org/10.1002/mma.8986
12. S. Liu, Z. Fu, S. Liu, Q. Zhao, Jacobi elliptic function expansion method and periodic wave solutions of nonlinear wave equations, *Phys. Lett. A*, **289** (2001), 69–74. https://doi.org/10.1016/S0375-9601(01)00580-1
13. S. A. Allahyani, H. U. Rehman, A. U. Awan, E. M. Tag-ElDin, M. U. Hassan, Diverse variety of exact solutions for nonlinear Gilson–Pickering equation, *Symmetry*, **14** (2022), 2151. https://doi.org/10.3390/sym14102151
14. D. Shi, H. U. Rehman, I. Iqbal, M. Vivas-Cortez, M. S. Saleem, X. Zhang, Analytical study of the dynamics in the double-chain model of DNA, **52** (2023), 106787. https://doi.org/10.1016/j.rinp.2023.106787
15. H. U. Rehman, A. U. Awan, E. M. Tag-ElDin, S. E. Alhazmi, M. F. Yassen, R. Haider, Extended hyperbolic function method for the (2 + 1)-dimensional nonlinear soliton equation, *Results Phys.*, **40** (2022), 105802. https://doi.org/10.1016/j.rinp.2022.105802
16. H. U. Rehman, M. A. Imran, N. Ullah, A. Akgül, Exact solutions of (2 + 1)dimensional Schrödinger's hyperbolic equation using different techniques, *Numer. Meth. Partial Differential Equations*, **39** (2020), 4575–4594. https://doi.org/10.1002/num.22644
17. M. U. Shahzad, H. U. Rehman, A. U. Awan, Z. Zafar, A. M. Hassan, I. Iqbal, Analysis of the exact solutions of nonlinear coupled Drinfeld–Sokolov–Wilson equation through ϕ^6-model expansion method, *Results Phys.*, **52** (2023), 106771. https://doi.org/10.1016/j.rinp.2023.106771
18. J. Sánchez-Curto, P. Chamorro-Posada, G. S. McDonald, Helmholtz solitons at nonlinear interfaces, *Optics Lett.*, **32** (2007), 1126–1128. https://doi.org/10.1364/OL.32.001126

19. P. Chamorro-Posada, G. S. McDonald, Spatial Kerr soliton collisions at arbitrary angles, *Phys. Rev. A*, **74** (2006), 036609. https://doi.org/10.1103/PhysRevE.74.036609

20. J. M. Christian, G. S. McDonald, R. J. Potton, P. Chamorro-Posada, Helmholtz solitons in power-law optical materials, *Phys. Rev. A*, **76** (2007), 033834. https://doi.org/10.1103/PhysRevA.76.033834

21. I. S. Hamad, K. K. Ali, Investigation of Brownian motion in stochastic Schrödinger wave equation using the modified generalized Riccati equation mapping method, *Opti. Quant. Electron.*, **56** (2024), 996. https://doi.org/10.1007/s11082-024-06865-y

22. S. Ibrahim, A. M. Ashir, Y. A. Sabawi, D. Baleanu, Realization of optical solitons from nonlinear Schrödinger equation using modified Sardar sub-equation technique, *Opti. Quant. Electron.*, **55** (2023), 617. https://doi.org/10.1007/s11082-023-04776-y

23. D. Chou, S. M. Boulaaras, H. U. Rehman, I. Iqbal, K. Khushi, Fractional nonlinear doubly dispersive equations: insights into wave propagation and chaotic behavior, *Alexandria Eng. J.*, **114** (2025), 507–525. https://doi.org/10.1016/j.aej.2024.11.097

24. M. Mirzazadeh, Q. Zhou, E. Zerrad, M. F. Mahmood, A. Biswas, M. Belic, Bifurcation analysis and bright soliton of generalized resonant dispersive nonlinear Schrödinger's equation, *Optoelectron. Adv. Mater., Rapid Commun.*, **9** (2015), 1342–1346.

25. A. H. Nayfeh, B. Balachandran, *Applied nonlinear dynamics: analytical, computational, and experimental methods*, John Wiley & Sons, 2008.

26. K. T. Alligood, T. D. Sauer, J. A. Yorke, *Chaos: an introduction to dynamical systems*, Springer, 1997. https://doi.org/10.1063/1.882006

27. S. Zambrano, E. Allaria, S. Brugioni, I. Leyva, R. Meucci, M. A. Sanjuán, et al., Numerical and experimental exploration of phase control of chaos, *Chaos*, **16** (2006), 013111. https://doi.org/10.1063/1.2161437

28. R. Meucci, S. Euzzor, E. Pugliese, S. Zambrano, M. R. Gallas, J. A. C. Gallas, Optimal phase-control strategy for damped-driven Duffing oscillators, *Phys. Rev. Lett.*, **116** (2016), 044101. https://doi.org/10.1103/PhysRevLett.116.044101

29. P. J. Martínez, S. Euzzor, J. A. C. Gallas, R. Meucci, R. Chacón, Identification of minimal parameters for optimal suppression of chaos in dissipative driven systems, *Sci. Rep.*, **7** (2017), 17988. https://doi.org/10.1038/s41598-017-17969-9

30. M. Ciofini, R. Meucci, F. Arecchi, Experimental control of chaos in a laser, *Phys. Rev. E*, **52** (1995), 94. https://doi.org/10.1103/PhysRevE.52.94